

Communication

Wideband E₀₀-E₁₀ Silicon Mode Converter Based on 180 nm CMOS Technology

Yan Xu ¹, Yang Gao ², Songyue Liu ¹, Tingyu Liu ¹, Xiaoqiang Sun ^{1,*} , Bo Tang ³, Peng Zhang ³ and Daming Zhang ¹ 

¹ Key Laboratory of Integrated Optoelectronics, College of Electronic Science & Engineering, Jilin University, Changchun 130012, China

² Zhejiang Lab, Hangzhou 311121, China

³ Institute of Microelectronics, Chinese Academy of Sciences, Beijing 100029, China

* Correspondence: sunxq@jlu.edu.cn; Tel.: +86-136-0430-4384

Abstract: Mode division multiplexing (MDM) is a promising technology for the capacity enlargement of the optical transmission network. As a key element in the MDM system, the mode converter plays an important role in signal processing. In this work, a wideband E₀₀-E₁₀ silicon mode converter constructed by Y-branch and cascaded multimode interference coupler is demonstrated. The theoretical mode crosstalk is less than -29.2 dB within the wavelength range from 1540 nm to 1600 nm. By 180 nm standard CMOS fabrication, the tested mode conversion efficiency of 91.5% and the crosstalk of -10.3 dB can be obtained at 1575.9 nm. The 3 dB bandwidth is over 60 nm. The proposed E₀₀-E₁₀ silicon mode converter is applicable in mode multiplexing.

Keywords: integrated optical devices; silicon waveguide; mode multiplexing; mode converter



Citation: Xu, Y.; Gao, Y.; Liu, S.; Liu, T.; Sun, X.; Tang, B.; Zhang, P.; Zhang, D. Wideband E₀₀-E₁₀ Silicon Mode Converter Based on 180 nm CMOS Technology. *Appl. Sci.* **2022**, *12*, 10688. <https://doi.org/10.3390/app122010688>

Academic Editor: Nunzio Cennamo

Received: 13 September 2022

Accepted: 20 October 2022

Published: 21 October 2022

Publisher's Note: MDPI stays neutral with regard to jurisdictional claims in published maps and institutional affiliations.



Copyright: © 2022 by the authors. Licensee MDPI, Basel, Switzerland. This article is an open access article distributed under the terms and conditions of the Creative Commons Attribution (CC BY) license (<https://creativecommons.org/licenses/by/4.0/>).

1. Introduction

Advanced by next-generation communicating and large-quantity signal processing, high-speed data transporting and large-capacity data handling are highly demanded. Due to the unique feature of photonics, various multiplexing methods, such as wavelength division multiplexing (WDM), polarization division multiplexing (PDM), as well as mode division multiplexing (MDM), are explored to enlarge the network capacity [1–7]. Except for the fiber optic network [8,9], the on-chip MDM transmission implemented by optical waveguide is investigated, too [10–12]. The mode signal can be processed by multimode interferometer (MMI) [13,14], directional coupler (DC) [15], Y junctions [16,17], micro-rings [12,18–20], and grating-assisted [21–23] and inversely designed structures [24]. The mode converter, as one key device in the MDM system, could realize the conversion to desired high-order modes within a certain bandwidth with features of high efficiency and low loss. As reported, the mode conversion is commonly implemented by DC or grating structures [25,26], however, the bandwidth is restrained by the intrinsic quality of DC, which limits the combination with WDM technologies to enlarge the capacity of data transmission.

In this paper, a wideband silicon E₀₀-E₁₀ mode converter is proposed. Finite difference beam propagation method (FD-BPM) calculations are used for the design optimization. The mode crosstalk is less than -29.2 dB within 1540–1600 nm. The theoretical design is experimentally implemented by 180 nm standard CMOS fabrication. The measured highest mode conversion efficiency is 91.5% at 1575.9 nm. The 3 dB bandwidth over 60 nm can be obtained. This E₀₀-E₁₀ silicon mode converter has possible utilization in fields of mode signal multiplexing.

2. Device Design

In MMI waveguides, the self-imaging effect could reproduce the input field profile in single or multiple images at periodic intervals along the propagation direction. Two scenarios exist in the MMI effect. One is the general interference, another case is the restricted interference. The beat length L_π can be described by

$$L_\pi = \frac{\pi}{\beta_0 - \beta_1} \approx \frac{4n_r w^2}{3\lambda_0} \quad (1)$$

where λ_0 is the operation wavelength, n_r is the refractive index of the core waveguide, and w is the width of the MMI coupler [27].

When one input waveguide is placed at the center of the MMI coupler, the distance L of M th N -fold images can be defined as

$$L = \frac{M}{4N}(3L_\pi). \quad (2)$$

For the MMI coupler with a certain length, and when only the fundamental mode or first-order mode is input, we have $M = N = 1$. The length of the MMI coupler L_{MMI} is

$$L_{\text{MMI}} = \frac{3}{4}L_\pi. \quad (3)$$

For instance, for the MMI coupler shown in Figure 1 below, two E_{00} modes with π phase difference are launched into the MMI section through two single modes. The interference between two E_{00} modes with different phases in the MMI waveguide leads to the E_{00} - E_{10} mode conversion. The first-order E_{10} mode will be excited at the output port on the right side of the MMI waveguide.

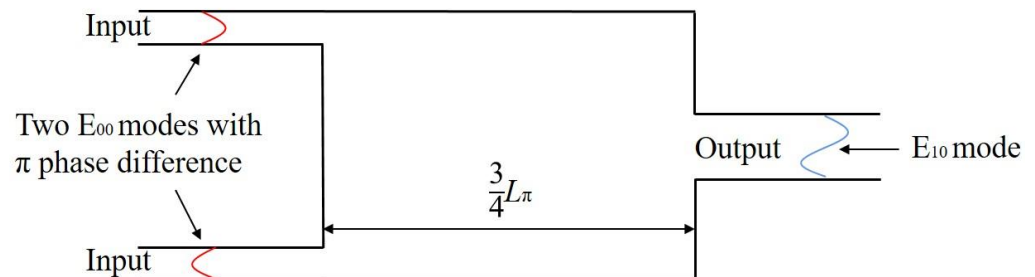


Figure 1. Diagram of MMI as E_{00} - E_{10} mode converter.

The proposed silicon E_{00} - E_{10} mode converter that is constructed by three sections of symmetric Y-branch 3 dB splitter, phase shifter (PS) waveguide, and 2×1 MMI coupler is shown in Figure 2a. Firstly, two E_{00} modes with the same mode power and phase are input into the PS waveguides via the 3 dB splitter. The π -phase difference would emerge between two E_{00} modes after passing through the PS waveguide constructed by cascaded tapered waveguides with different lengths. The interference between two E_{00} modes with different phases in the MMI coupler leads to the E_{00} - E_{10} mode conversion. Figure 2b shows the cross-sectional view of the silicon waveguide.

When the silicon core thickness is fixed to 220 nm, the variation in effective indices (n_{eff}) of two modes with the silicon core width is illustrated in Figure 3a. To support the E_{00} mode, the width of the input waveguide (w_1) is chosen as 0.4 μm . We set the width of the output waveguide (w_3) as 0.8 μm to support both the E_{00} mode and E_{10} mode. For getting π -phase difference, it is necessary to strictly manipulate the dimensional parameters of PS waveguides. With FD-BPM calculating, the width of the Y-branch 3 dB coupler (w_1) is set to be $w_1 = 0.4 \mu\text{m}$, and PS waveguides (w_2) are set to be $w_2 = 0.28 \mu\text{m}$ to support E_{00} mode. Additionally, the lengths of different tapered waveguides l_1 , l_2 , and l_3 are selected to be 3.6 μm , 12.4 μm , and 8 μm , respectively.

Here, the width of MMI coupler w_{MMI} is chosen to be $3.3 \mu\text{m}$, thereby, the beat length L_{π} is calculated to be $32.5 \mu\text{m}$ at 1550 nm according to Equation (1). The length of MMI coupler that can be calculated by Equation (3) is optimized to be $25.3 \mu\text{m}$ for a compact size. With above parameters, the mode field distribution of the proposed mode converter at 1550 nm is shown in Figure 3b.

To be mentioned, the length of the Y-branch is chosen to be $25 \mu\text{m}$, the length of the taper that connects the Y-branch and PS is chosen to be $8 \mu\text{m}$, and the length of the straight waveguide that connects PS and MMI is chosen to be $5 \mu\text{m}$. These parameters are compromise choices after comprehensive consideration of optical loss and device size.

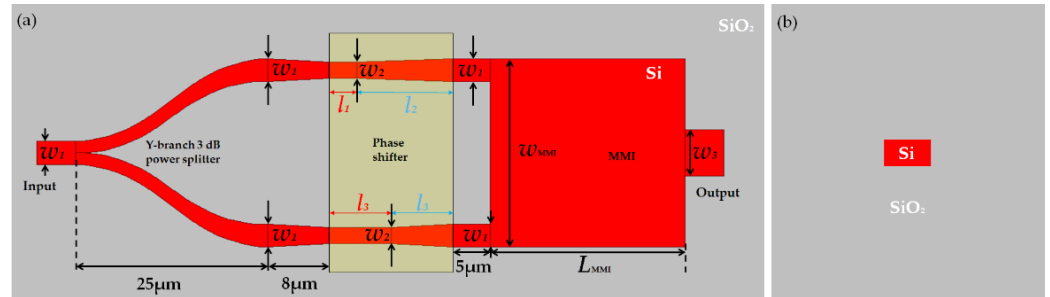


Figure 2. Schematic diagram of the (a) E_{00} - E_{10} silicon mode converter, and (b) cross-section of silicon waveguide.

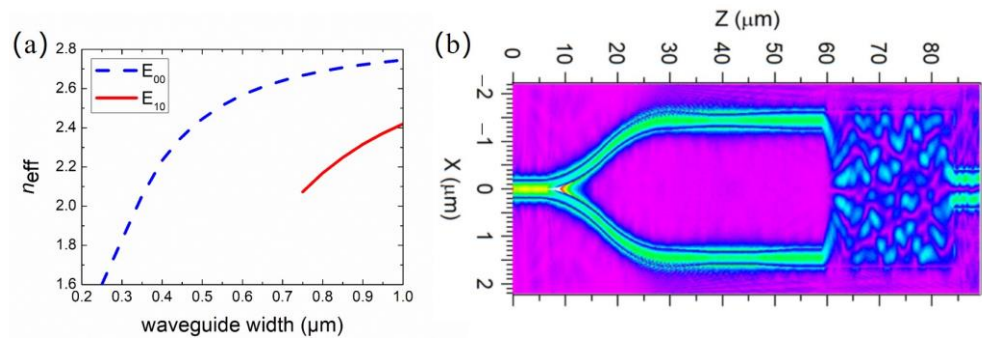


Figure 3. (a) The effective indices of E_{00} and E_{10} modes as a function of core layer waveguide width with 220 nm silicon core thickness, (b) mode field distribution of mode converter at 1550 nm .

The normalized transmission spectra and conversion efficiency of E_{00} mode and E_{10} mode investigated by FD-BPM calculations under $25 \text{ }^\circ\text{C}$ room temperature is presented in Figures 4 and 5, respectively. The minimum mode crosstalk of -41.7 dB occurs at 1566 nm . Moreover, the crosstalk is less than -29.2 dB within the wavelength range from 1540 nm to 1600 nm , which implies the conversion efficiency of the E_{00} to E_{10} mode is larger than 87.9% within the interested wavelength range. The maximum mode conversion is around 99.6% happened at 1575 nm . The normalized transmission (T) as dB can be represented by Equation (4), where a is the transmittance of the corresponding mode.

$$T = 10\lg(a) \tag{4}$$

To confirm the temperature characteristic of the proposed mode converter, the E_{00} to E_{10} mode conversion at different temperatures was investigated. When the thermo-optic coefficient of silicon is $1.88 \times 10^{-4} / \text{K}$ [28], the simulated conversion efficiency as a function of wavelength is as shown in the Figure 6. It can be seen that no obvious bandwidth change happens. However, when the operation temperature varies from $25 \text{ }^\circ\text{C}$ to $40 \text{ }^\circ\text{C}$, the maximum conversion efficiency happens at 1575 nm , 1573 nm , 1572 nm , and 1571 nm , respectively. The blueshift of maximum conversion efficiency with the increment of temperature can be observed. Fortunately, the 3 dB bandwidths are all larger than 60 nm

at temperatures of 25 °C, 30 °C, 35 °C, and 40 °C, which proves the favorable temperature stability of the proposed device. This phenomenon can be explained by the unremarkable size change of the silicon waveguide and the limited variation in the effective refractive index, which is favorable to stable mode conversion.

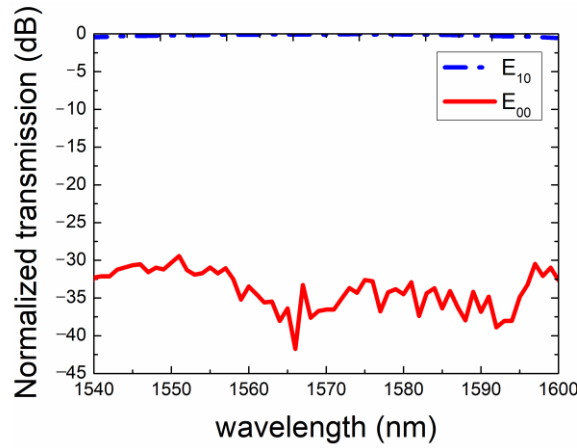


Figure 4. Normalized transmission of the proposed E_{00} - E_{10} mode converter when the wavelength varies from 1540 nm to 1600 nm.

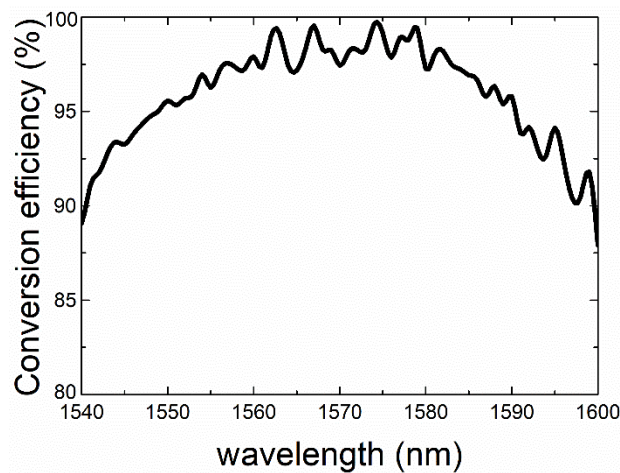


Figure 5. Conversion efficiency as a function of wavelength from 1540 nm to 1600 nm.

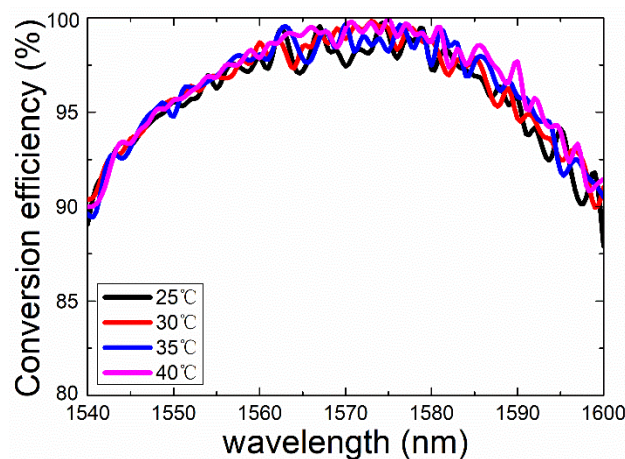


Figure 6. Simulated mode conversion as a function of wavelength at different temperatures.

3. Results and Discussion

The proposed mode converter was fabricated on silicon on insulator (SOI) wafer with 180 nm CMOS technology. The thicknesses of the top silicon and buried silica layers were 220 nm and 3 μm , respectively. By deep ultraviolet (UV) photolithography, the waveguide patterns were transferred onto the photoresist. After development, the unprotected top silicon was removed by coupled plasma etching, which offers the rectangular shape silicon waveguides. Thereafter, 1 μm -thick silica was deposited by PECVD onto the SOI wafer as the top cladding. Figure 7 shows the microscope image ($\times 1000$ times) of the mode converter. The light from the fiber is coupled into the Y-branch through the grating coupler. Thereafter, the split modes pass through the phase shifters and interfere in the MMI section. The light output from the grating coupler is on the right side. To be mentioned, the layout of Y-branch 3 dB splitter is modified to satisfy the design rule of 180 nm CMOS technology.

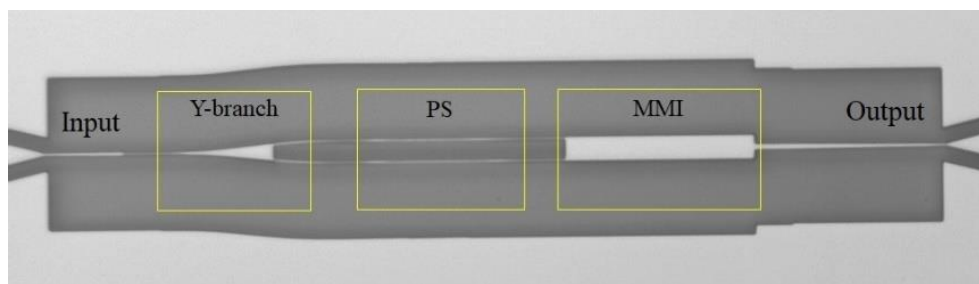


Figure 7. Microscope image ($\times 1000$ times) of fabricated silicon E_{00} - E_{10} mode converter.

The schematic diagram of measurement setup is shown in Figure 8. Figure 9 shows the picture that the converter is under test. After passing through the polarization controller, the light from the tunable laser source is coupled into the 3 dB splitter by a grating coupler via the single mode fiber (SMF). Since the converted E_{10} higher mode is hard to directly observe through the single mode grating coupler, it is first filtered through a tapered waveguide. In this way, only the fundamental E_{00} mode can pass and be collected by another SMF via the vertical grating coupler. Through a fiber power splitter, the obtained E_{00} mode is coupled into the optical spectrum analyzer (OSA) (90%) and the optical power meter (OPM) (10%), respectively.

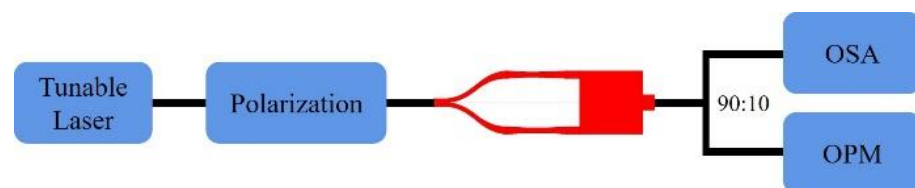


Figure 8. Schematic diagram of E_{00} - E_{10} mode converter measurement setup.

To find out the loss of the proposed mode converter, referential waveguides with different lengths are fabricated together with the mode converter. These referential waveguides consist of two identical grating couplers and a straight single mode waveguide. The propagation loss single mode silicon waveguide is confirmed to be ~ 1 dB/cm. Two grating couplers-induced loss can be deduced by removing the single mode waveguide-induced loss from the measured insertion loss of referential waveguide. Figure 10 shows the grating coupler-induced loss as the function of the optical wavelength. It can be seen that input/output gratings-induced loss within the wavelength range from 1540 to 1600 nm is lower than -25 dB. The minimum value of -25.06 dB happens at 1575.9 nm.

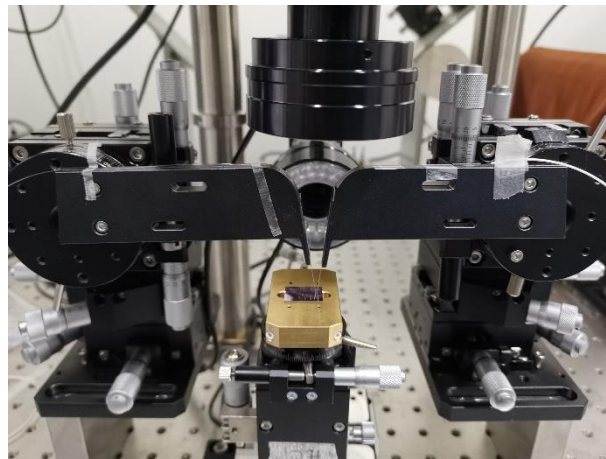


Figure 9. Experimental test system with vertical grating couplers.

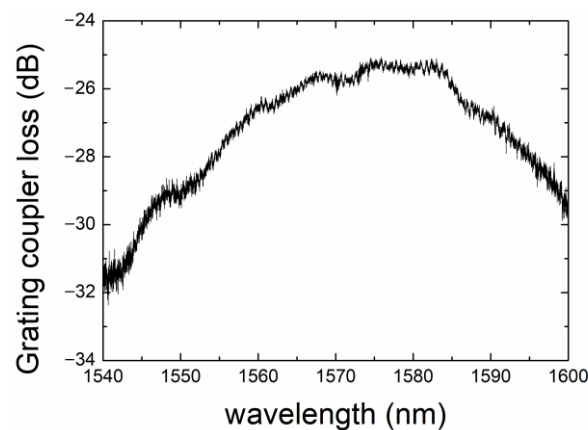


Figure 10. Measured optical loss induced by the input and output grating couplers.

The measured transmission spectrum and conversion efficiency of the mode converter within the wavelength range from 1540 nm to 1600 nm is shown in Figures 11 and 12, respectively. It can be seen that the highest conversion efficiency of 91.5% occurred at 1575.9 nm, and the corresponding mode crosstalk is -10.3 dB. The conversion efficiency in percent (E_p) and dB (E_d) are calculated by Equation (5) and Equation (6), respectively. Here, b is the propagation loss of the E_{00} mode in the dB scale.

$$E_p = (1 - 10^{0.1b}) \times 100\% \quad (5)$$

$$E_d = 10\lg(1 - 10^{0.1b}) \quad (6)$$

The 3 dB bandwidth is confirmed to be over 60 nm according to the measured E_{10} mode spectrum in Figure 11. The fluctuation of transmission is due to the overclose distance between the input/output fiber and the grating coupler, which may lead to the instability caused by the Fabry–Pérot cavity. Therefore, the distance between the input/output fibers and the chip surface is supposed to be well controlled to guarantee the accuracy of the measurement. To be noted, the transmission is only characterized at 25 °C due to the limitation of the measurement setup.

Compared with the simulated results in Figure 4, the E_{10} mode conversion shows good matching to experimental results. However, the measured mode crosstalk deviates from the theoretical expectations apparently. This partly results from the unavoidable fabrication errors. Due to the rules of 180 nm CMOS technology, compromises have to be made in the waveguide layout design. The change in waveguide dimensions compared to the ideal size inevitably affects the phase difference between the two branch arms. In the

MMI coupler, the phase difference error will lead to the deviation of mode interference from theoretical expectations. Not all the E_{00} mode was converted to E_{10} mode. Partial E_{00} mode power remains at the output, which deteriorates the mode crosstalk within the interested wavelength range. This effect first degenerates with the increment of the wavelength, then becomes serious again at longer wavelengths.

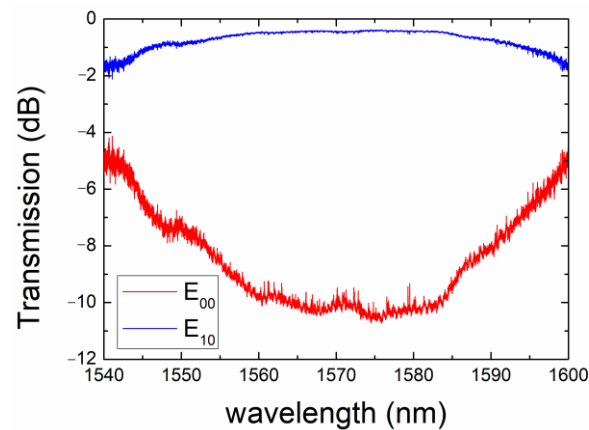


Figure 11. Measured transmission spectrum of fabricated mode converter in 1540–1600 nm.

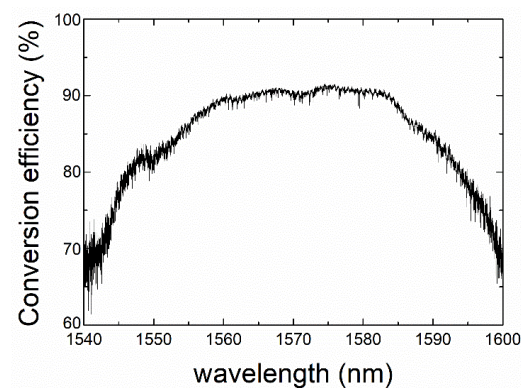


Figure 12. Measured E_{00} - E_{10} conversion efficiency of fabricated mode converter in 1540–1600 nm.

To demonstrate the proposed mode converter more clearly, performance comparisons between the reported E_{00} - E_{10} mode converters and this work are shown in Table 1. All referential experimental results are based on the SOI technology. The inversely designed mode converter shows the lowest mode crosstalk [29], while the mode converter, based on the slot waveguide, has the smallest size and the lowest insertion loss [30]. The photonic crystal waveguide-based converter exhibits balanced performances [31]. In comparison, the proposed work shows the moderate insertion loss and mode crosstalk. Though the largest size, the broadest bandwidth and lower E_{10} mode insert loss promise favorable potentials in wideband operation.

Table 1. Comparison the proposed silicon E_{00} - E_{10} mode converter with reported works.

Ref.	Footprint (μm^2)	Insert Loss (dB)	Crosstalk (dB)	BW (nm)	Structure	Materials
[29]	2×2	2.2	-16.2	40	Inversely design	SOI
[30]	0.8×1.2	<1.2	/	50	Slots waveguide	SOI
[31]	6.3×3.6	2	-12	43	Photonic crystal waveguide	SOI
This work	3.3×79.3	0.4–2	>-10.3	>60	PS + MMI	SOI

4. Conclusions

In this work, a wideband silicon mode converter based on E_{00} - E_{10} is theoretically proposed and experimentally demonstrated. With FD-BPM calculations, the simulated mode crosstalk is less than -29.2 dB in 1540–1600 nm. The standard 180 nm CMOS technology is applied in the fabrication of designed device, instead of the E-beam lithography. The best mode conversion, with an efficiency of 91.5%, is observed at 1575.9 nm. The comparatively wide 3 dB bandwidth of over 60 nm offers the proposed great potential of on-chip multiplexing systems in future.

Author Contributions: Conceptualization and resources, D.Z.; formal analysis and investigation, Y.X.; validation, Y.G.; data curation, S.L. and T.L.; funding acquisition, B.T.; writing—review and editing, X.S.; project administration, P.Z.; All authors have read and agreed to the published version of the manuscript.

Funding: This study was supported by the National Key Research and Development Program of China (2019YFB2203003).

Institutional Review Board Statement: Not applicable.

Informed Consent Statement: Not applicable.

Data Availability Statement: Not applicable.

Conflicts of Interest: The authors declare no conflict of interest.

References

1. Chun, H.; Rajbhandari, S.; Faulkner, G.; Tsonev, D.; Enyuan, X.; McKendry, J.J.D.; Gu, E.; Dawson, M.D.; O'Brien, D.C.; Haas, H. LED based wavelength division multiplexed 10 Gb/s visible light communications. *J. Light. Technol.* **2016**, *34*, 3047–3052. [[CrossRef](#)]
2. Xing, F.; Chen, H.; Xie, S.; Yao, J. Ultrafast surface imaging with an increased spatial resolution based on polarization-division multiplexing. *J. Light. Technol.* **2015**, *33*, 396–402. [[CrossRef](#)]
3. Zhang, Y.; Pan, S. Photonics-based multi-function analog signal processor based on a polarization division multiplexing Mach-Zehnder modulator. *Opt. Lett.* **2017**, *42*, 5034–5037. [[CrossRef](#)]
4. Goossens, J.; Yousefi, M.; Jaouen, Y.; Hafermann, H. Polarization-division multiplexing based on the nonlinear Fourier transform. *Opt. Express* **2017**, *25*, 26437–26452. [[CrossRef](#)]
5. Xiao, H.; Liu, Z.; Han, X.; Yang, J.; Ren, G.; Mitchell, A.; Tian, Y. On-chip reconfigurable and scalable optical mode multiplexer/demultiplexer based on three-waveguide-coupling structure. *Opt. Express* **2018**, *26*, 22366–22377. [[CrossRef](#)]
6. Gao, Y.; Xu, Y.; Ji, L.; Sun, X.; Wang, F.; Wang, X.; Wu, Y.; Zhang, D. Scalable compact mode (de)multiplexer based on asymmetric Y-junctions. *Opt. Commun.* **2019**, *438*, 34–38. [[CrossRef](#)]
7. Driscoll, J.B.; Chen, C.P.; Grote, R.R.; Souhan, B.; Dadap, J.I.; Stein, A.; Lu, M.; Bergman, K.; Osgood, R.M. A 60 Gb/s MDM-WDM Si photonic link with <0.7 dB power penalty per channel. *Opt. Express* **2014**, *22*, 18543–18555.
8. Berdagué, S. Mode division multiplexing in optical fibers. *Appl. Opt.* **1982**, *21*, 1950. [[CrossRef](#)]
9. Jiang, S.; Ma, L.; Zhang, Z.; Xu, X.; Wang, S.; Du, J.; Yang, C.; Tong, W.; He, Z. Design and characterization of ring-assisted few-mode fibers for weakly coupled mode-division multiplexing transmission. *J. Light. Technol.* **2018**, *36*, 5547–5555. [[CrossRef](#)]
10. Ding, Y.; Xu, J.; Da Ros, F.; Huang, B.; Ou, H.; Peucheret, C. On-chip two-mode division multiplexing using tapered directional coupler-based mode multiplexer and demultiplexer. *Opt. Express* **2013**, *21*, 10376–10382. [[CrossRef](#)] [[PubMed](#)]
11. Dai, D.; Li, C.; Wang, S.; Wu, H.; Shi, Y.; Wu, Z.; Gao, S.; Dai, T.; Yu, H.; Tsang, H. 10-channel mode (de)multiplexer with dual polarizations. *Laser Photon. Rev.* **2018**, *12*, 1700109. [[CrossRef](#)]
12. Luo, L.W.; Ophir, N.; Chen, C.; Gabrielli, L.; Poitras, C.; Bergmen, K.; Lipson, M. WDM-compatible mode-division multiplexing on a silicon chip. *Nat. Commun.* **2014**, *5*, 3069. [[CrossRef](#)] [[PubMed](#)]
13. Li, Y.; Li, C.; Li, C.; Cheng, B.; Xue, C. Compact two-mode (de)multiplexer based on symmetric Y-junction and multimode interference waveguides. *Opt. Express* **2014**, *22*, 5781–5786. [[CrossRef](#)] [[PubMed](#)]
14. Gao, Y.; Sun, X.; Li, P.; Zhang, D. Polymer mode selecting switch based on cascaded MMI couplers. *IEEE Photon. Technol. Lett.* **2021**, *33*, 147–150. [[CrossRef](#)]
15. Sun, Y.; Xiong, Y.; Ye, W.N. Experimental demonstration of a two-mode (de)multiplexer based on a taper-etched directional coupler. *Opt. Lett.* **2016**, *41*, 3743–3746. [[CrossRef](#)] [[PubMed](#)]
16. Chen, W.; Wang, P.; Yang, T.; Wang, G.; Dai, T.; Zhang, Y.; Zhou, L.; Jiang, X.; Yang, J. Silicon three-mode (de)multiplexer based on cascaded asymmetric Y junctions. *Opt. Lett.* **2016**, *41*, 2851–2854. [[CrossRef](#)]
17. Zhang, Z.; Yu, Y.; Fu, S. Broadband on-chip mode-division multiplexer based on adiabatic couplers and symmetric Y-junction. *IEEE Photonics J.* **2017**, *9*, 6600406.

18. Jia, H.; Fu, X.; Zhou, T.; Zhang, L.; Yang, S.; Yang, L. Mode-selective modulation by silicon microring resonators and mode multiplexers for on-chip optical interconnect. *Opt. Express* **2019**, *27*, 2915–2925. [[CrossRef](#)]
19. Xiao, H.; Zhang, Z.; Yang, J.; Han, X.; Chen, W.; Ren, G.; Mitchell, A.; Yang, J.; Gao, D.; Tian, Y. On-chip scalable mode-selective converter based on asymmetrical micro-racetrack resonators. *Nanophotonics* **2020**, *9*, 1447. [[CrossRef](#)]
20. Ye, M.; Yu, Y.; Chen, G.; Luo, Y.; Zhang, X. On-chip WDM mode-division multiplexing interconnection with optional demodulation function. *Opt. Express* **2015**, *23*, 32130–32138. [[CrossRef](#)]
21. Qiu, H.; Yu, H.; Hu, T.; Jiang, G.; Shao, H.; Yu, P.; Yang, J.; Jiang, X. Silicon mode multi/demultiplexer based on multimode grating-assisted couplers. *Opt. Express* **2013**, *21*, 17904–17911. [[CrossRef](#)] [[PubMed](#)]
22. Gui, C.; Gao, Y.; Zhang, Z.; Wang, J. On-chip silicon two-mode (de)multiplexer for OFDM/OQAM data transmission based on grating-assisted coupler. *IEEE Photon. J.* **2015**, *7*, 7905807. [[CrossRef](#)]
23. He, Y.; Zhang, Y.; Wang, H.; Sun, L.; Su, Y. Design and experimental demonstration of a silicon multi-dimensional (de)multiplexer for wavelength-, mode- and polarization-division (de)multiplexing. *Opt. Lett.* **2020**, *45*, 2846–2849. [[CrossRef](#)] [[PubMed](#)]
24. Xie, H.; Liu, Y.; Wang, S.; Wang, Y.; Yao, Y.; Song, Q.; Du, J.; He, Z.; Xu, K. Highly compact and efficient four-mode multiplexer based on pixelated waveguides. *IEEE Photon. Technol. Lett.* **2020**, *32*, 166–169. [[CrossRef](#)]
25. Wang, J.; Zhai, Y.; Mao, J.; Lu, Y.; Xu, J.; Dai, D. Silicon-nanowire-based optical hybrid with insensitive operation for TE/TM states of polarization. *Opt. Commun.* **2017**, *385*, 124–129. [[CrossRef](#)]
26. Wang, H.; Zhang, Y.; He, Y.; Zhu, Q.; Sun, L.; Su, Y. Compact silicon waveguide mode converter employing dielectric metasurface structure. *Adv. Opt. Mater.* **2019**, *7*, 1801191. [[CrossRef](#)]
27. Gao, Y.; Zhang, D.; Xu, Y.; Fan, X.; Wang, F.; Sun, X. Ultra-broadband polymer E_{00}/E_{10} mode converter. *Opt. Commun.* **2022**, *508*, 127715. [[CrossRef](#)]
28. Guzman-Chavez, A.D.; Vargas-Rodriguez, E. Enhanced thermally tunable optical filter and its applications in Erbium-doped fiber lasers. *IEEE Photon. Technol. Lett.* **2020**, *32*, 297–300. [[CrossRef](#)]
29. Wang, T.; Guo, H.; Chen, H.; Yang, J.; Jia, H. Ultra-compact reflective mode converter based on a silicon subwavelength structure. *Appl. Opt.* **2020**, *59*, 2754–2758. [[CrossRef](#)]
30. Zhao, Y.; Guo, X.; Zhang, Y.; Xiang, J.; Wang, K.; Wang, H.; Su, Y. Ultra-compact silicon mode-order converters based on dielectric slots. *Opt. Lett.* **2020**, *45*, 3797–3800. [[CrossRef](#)]
31. Frandsen, L.H.; Elesin, Y.; Frelsen, L.F.; Mitrovic, M.; Ding, Y.H.; Sigmund, O.; Yvind, K. Topology optimized mode conversion in a photonic crystal waveguide fabricated in silicon-on-insulator material. *Opt. Express* **2014**, *22*, 8525–8532. [[CrossRef](#)] [[PubMed](#)]